






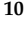



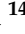






Article

Rainfall in the Urban Area and Its Impact on Climatology and Population Growth

Lua da Silva Monteiro ¹, José Francisco de Oliveira-Júnior ¹, Bushra Ghaffar ², Aqil Tariq ^{3,4,*}, Shujing Qin ^{5,*,†}, Faisal Mumtaz ^{6,7}, Washington Luiz Félix Correia Filho ⁸, Munawar Shah ⁹, Alexandre Maniçoba da Rosa Ferraz Jardim ¹⁰, Marcos Vinícius da Silva ¹⁰, Dimas de Barros Santiago ¹¹, Heliofábio Gomes Barros ¹, David Mendes ¹², Marcel Carvalho Abreu ¹³, Amaury de Souza ¹⁴, Luiz Cláudio Gomes Pimentel ¹⁵, Jhon Lennon Bezerra da Silva ¹⁶, Muhammad Aslam ¹⁷ and Alban Kuriqi ^{18,19}

- ¹ Institute of Atmospheric Sciences (ICAT), Federal University of Alagoas (UFAL), Maceió 57072-260, Alagoas, Brazil
- ² Department of Environmental Science, Faculty of Basic and Applied Sciences, International Islamic University, Islamabad 44000, Pakistan
- ³ Department of Wildlife, Fisheries, and Aquaculture, Mississippi State University, 775 Stone Boulevard, Starkville, MS 39762, USA
- ⁴ State Key Laboratory of Information Engineering in Surveying, Mapping and Remote Sensing, Wuhan University, Wuhan 430072, China
- ⁵ State Key Laboratory of Water Resources and Hydropower Engineering Science, Wuhan University, Wuhan 430072, China
- ⁶ State Key Laboratory of Remote Sensing Sciences, Aerospace Information Research Institute, Chinese Academy of Sciences, Beijing 100101, China
- ⁷ University of Chinese Academy of Sciences (UCAS), Beijing 101408, China
- ⁸ Institute of Mathematics, Statistics, and Physics (IMEF), Federal University of Rio Grande (FURG), Rio Grande 96203-900, Rio Grande do Sul, Brazil
- ⁹ Department of Space Science, Space Education and GNSS Lab, National Center for GIS and Space Application, Institute of Space Technology, Islamabad 44000, Pakistan
- ¹⁰ Department of Agricultural Engineering, Federal Rural University of Pernambuco (UFRPE), Dom Manoel de Medeiros Avenue, SN, Dois Irmãos, Recife 52171-900, Pernambuco, Brazil
- ¹¹ Postgraduate Program in Meteorology, Academic Unit of Atmospheric Sciences (UACA), Federal University of Campina Grande (UFCG), Campina Grande 58429-140, Paraíba, Brazil
- ¹² Post-Graduate Program in Aerospace Engineering—PPGEA, Federal University of Rio Grande do Norte—UFRN, Campus Universitário Lagoa Nova, Natal 59078-970, Rio Grande do Norte, Brazil
- ¹³ Department of Environmental Sciences, Forestry Institute, Federal Rural University of Rio de Janeiro, Rod. BR 465, Km 07, Seropédica 23890-000, Rio de Janeiro, Brazil
- ¹⁴ Physics Institute, Federal University of Mato Grosso do Sul, C.P. 549, Campo Grande 79070-900, Mato Grosso do Sul, Brazil
- ¹⁵ Department of Meteorology, Geoscience Institute (IGEO), Federal University of Rio de Janeiro (UFRJ), Rio de Janeiro 21941-916, Rio de Janeiro, Brazil
- ¹⁶ National Institute of the Semi-Arid (INSA), Núcleo de Gestão da Informação e Popularização da Ciência, Campina Grande 58434-700, Paraíba, Brazil
- ¹⁷ School of Computing Engineering and Physical Sciences, University of West of Scotland, Paisley G72 0LH, UK
- ¹⁸ CERIS, Instituto Superior Técnico, Universidade de Lisboa, 1049-001 Lisboa, Portugal
- ¹⁹ Civil Engineering Department, University for Business and Technology, 10000 Pristina, Kosovo
- * Correspondence: at2139@msstate.edu or aqiltariq@whu.edu.cn (A.T.); shujing.qin@whu.edu.cn (S.Q.)
- † Shujing Qin act as co-corresponding authors.



Citation: da Silva Monteiro, L.; de Oliveira-Júnior, J.F.; Ghaffar, B.; Tariq, A.; Qin, S.; Mumtaz, F.; Correia Filho, W.L.F.; Shah, M.; da Rosa Ferraz Jardim, A.M.; da Silva, M.V.; et al. Rainfall in the Urban Area and Its Impact on Climatology and Population Growth. *Atmosphere* **2022**, *13*, 1610. <https://doi.org/10.3390/atmos13101610>

Academic Editors: Guocan Wu and Yuna Mao

Received: 2 September 2022

Accepted: 26 September 2022

Published: 1 October 2022

Publisher's Note: MDPI stays neutral with regard to jurisdictional claims in published maps and institutional affiliations.



Copyright: © 2022 by the authors. Licensee MDPI, Basel, Switzerland. This article is an open access article distributed under the terms and conditions of the Creative Commons Attribution (CC BY) license (<https://creativecommons.org/licenses/by/4.0/>).

Abstract: Due to the scarcity of studies linking the variability of rainfall and population growth in the capital cities of Northeastern Brazil (NEB), the purpose of this study is to evaluate the variability and multiscale interaction (annual and seasonal), and in addition, to detect their trends and the impact of urban growth. For this, monthly rainfall data between 1960 and 2020 were used. In addition, the detection of rainfall trends on annual and seasonal scales was performed using the Mann–Kendall (MK) test and compared with the phases of El Niño–Southern Oscillation (ENSO) and Pacific Decadal Oscillation (PDO). The relationship between population growth data and rainfall data for different decades was established. Results indicate that the variability of multiscale urban rainfall

is directly associated with the ENSO and PDO phases, followed by the performance of rain-producing meteorological systems in the NEB. In addition, the anthropic influence is shown in the relational pattern between population growth and the variability of decennial rainfall in the capitals of the NEB. However, no capital showed a significant trend of increasing annual rainfall (as in the case of Aracaju, Maceió, and Salvador). The observed population increase in the last decades in the capitals of the NEB and the notable decreasing trend of rainfall could compromise the region's water security. Moreover, if there is no strategic planning about water bodies, these changes in the rainfall pattern could be compromising.

Keywords: NEB; urban rainfall; meteorological systems; population growth

1. Introduction

Northeastern Brazil (NEB) has a high spatiotemporal variability of rainfall, with a direct influence on various human activities, mainly in the agricultural sector, tourism, and industry, as well as on the dynamics and phytophysiology of existing biomes [1–3]. Due to its geographic location, several multiscale meteorological systems, from local to large scale, contribute to rainfall dynamics in the NEB [4–6].

Different rainfall regimes for sub-regions of the NEB (East, North, and South) suggest that more than one mechanism is responsible for its spatiotemporal variability [7–9]. Among the large-scale mechanisms that organize convection on a synoptic scale are the Intertropical Convergence Zone (ITCZ), the South Atlantic Convergence Zone (SACZ), Frontal Systems (FS), High-Level Cyclonic Vortices (HLCV), South Atlantic Subtropical High (SASH), and the Madden–Julian Oscillation (MJO) [10–14]. Mesoscale mechanisms include Trade Wave Disturbances (TWD), Easterly Wave Disturbances (EWD), Mesoscale Convective Complexes (MCC), and sea/land, valley/mountain, and lake/lagoon circulations [5,13,15]. Orographic circulations and local convection constitute microscale phenomena [8].

In addition, there are modes of climate variability, for example, the El Niño–Southern Oscillation (ENSO) [3,5] and the Atlantic Dipole, currently called Interhemispheric Gradient of Atlantic Sea Surface Temperature (GIASST) [11], which influences the interannual variability of rainfall in the NEB [12,16,17]. Studies show that in El Niño/La Niña years, the NEB has less and/or more annual rainfall compared to climatology [3,6,7]. Another important mode of climate variability in the NEB is the Pacific Decadal Oscillation (PDO), which, in turn, is directly linked to the ENSO phases. The PDO refers to the ocean–atmosphere interaction in the Pacific Ocean, which is dominant on the inter-annual scale and influences the NEB rainfall distribution [11,18].

In addition, extreme coastal rainfall events are common in the NEB capital cities [19]. When associated with cities with precarious infrastructure and unplanned growth, these events result in floods, flash flood overflows, and an increase in waterborne diseases (dengue, zika, chikungunya, and leptospirosis) [20,21].

The rapid and disorderly expansion of urban centers leads to the waterproofing of extensive areas and urban drainage problems [22,23]. It is known that increased soil impermeability due to urbanization impacts rainfall in urban areas and the local hydrological system [24] and also causes changes in rainfall intensity and frequency patterns [25–27]. Urban rainfall affects daily human activities and the environment [28].

Previously, Sousa et al. [29] estimated the risks of extreme rainfall in the nine capitals of the NEB in the period from 1910 to 2012 and found that the large-scale mechanisms that operate in the NEB, in the first four months of the year, HLCV and ITCZ, can be intensified by local effects and cause the intensity of the rainfall, mainly in the coast and in the Agreste region to the central region of the NEB. Recently, Da Silva et al. [30] analyzed rainfall in the eastern portion of the NEB (ENEB) via the Standardized Precipitation Index (SPI) and Wavelet Analysis from 1961 to 2014 and found that the occurrence of droughts was higher in all capitals, however, extreme rainfall events became frequent. Additionally, according

to the authors, extreme weather events (rainy or dry) occur most of the time, apparently influenced by ENSO phases. The presence of timescales related to ENSO, Atlantic Dipole mode, sunspot cycle, and PDO was also identified in all capitals in this study.

To date, few studies have been carried out with the assessment of spatiotemporal variability and rainfall trends in the capitals of the NEB [e.g., 5, 11]; the existing ones are summarized in studies [31] or, when in their entirety, the lack of their socio-environmental impacts, especially in the last 60 years. Therefore, the objective of this study was to evaluate the variability of urban rainfall on a multiscale (annual and seasonal) in the capitals of the NEB, with emphasis on the identification of the meteorological systems responsible for the occurrence of the seasonality of urban rainfall and the detection of its trends.

2. Materials and Methods

2.1. Study Area

The NEB is located between the parallels $01^{\circ}02'30''$ N and $18^{\circ}20'07''$ S and between the longitudes of $34^{\circ}47'30''$ and $48^{\circ}45'24''$ west (W) of Greenwich. The regions under study are the capitals of the NEB: Aracaju (SE), Fortaleza (CE), João Pessoa (PB), Maceió (AL), Natal (RN), Recife (PE), Salvador (BA), São Luís (MA), and Teresina (PI), as shown in Figure 1. Table 1 shows the population of the capitals of the NEB based on the censuses of the Brazilian Institute of Geography and Statistics (IBGE) [32].

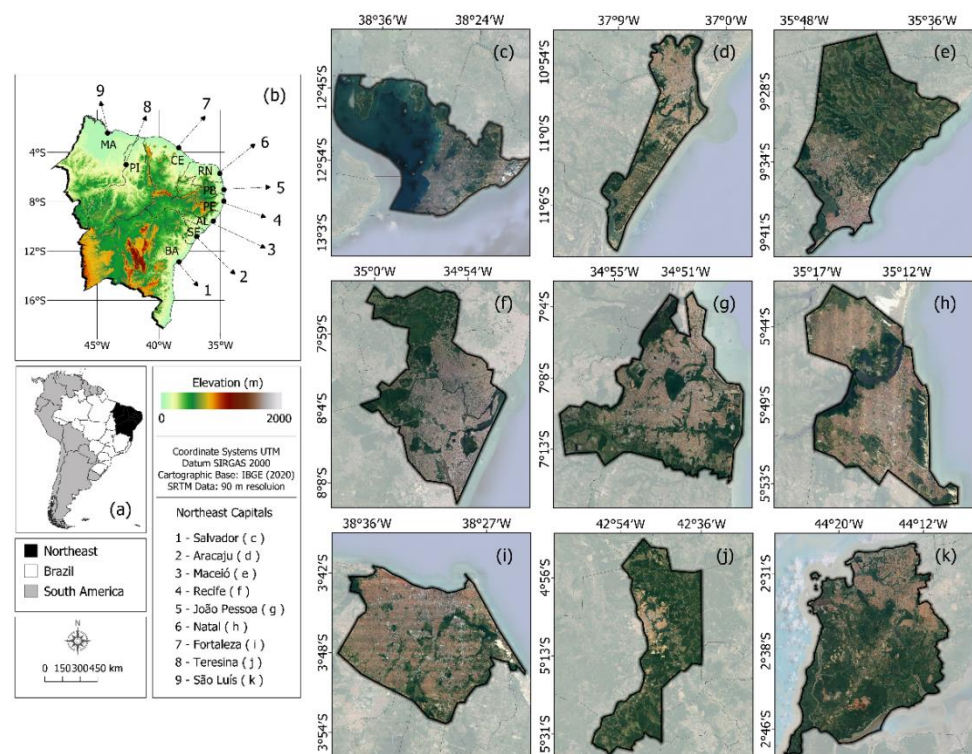


Figure 1. Location of the study area, with emphasis on the nine capitals and the elevation (m) of the NEB. Legend: (a) Brazil, (b) elevation in Northeast region, (c) Salvador, (d) Aracaju, (e) Maceió, (f) Recife, (g) João Pessoa, (h) Natal, (i) Fortaleza, (j) Teresina and (k) São Luís.

Table 1. Estimated population for NEB capitals. Source: [32].

Capitals	Population (1991)	Population (2000)	Population (2010)	Population (2020)
Aracaju	404,828	451,027	571,149	664,908
Fortaleza	1,708,741	2,139,372	2,452,185	2,686,612
João Pessoa	484,291	594,968	723,515	817,511
Maceió	699,760	806,167	932,748	1,025,360
Natal	606,276	699,339	803,739	890,480
Recife	1,335,684	1,388,193	1,537,704	1,653,461
Salvador	2,075,392	2,331,612	2,675,656	2,886,698
São Luís	781,374	855,442	1,014,837	1,108,975
Teresina	591,164	703,796	814,230	868,075

2.2. Rainfall Data and Evaluation

We are referring for the data of 9 stations for rainfall and population evaluation in various cities of NEB according to the spatial distribution of Figure 1 and Table 2. The stations belonging to the hydrometeorological network of ANA—Agência Nacional das Águas (ANA, 2021) are obtained via the HidroWeb platform at the following electronic address: <http://www.ana.gov.br>, accessed on 8 August 2022. The period comprises the years 1960 to 2020.

Table 2. The detail about the parameters from 9 different stations.

ID	Capitals	Lat. (°)	Long. (°)	Alt. (m)	Average Rainfall (mm)	Percentage of Failures ** (%)
1	Aracaju	−10.95	−37.05	3.68	1403.13	16.12
2	Fortaleza	−3.82	−38.54	29.89	1607.61	20.08
3	João Pessoa	−7.10	−34.85	9.67	1906.07	10.79
4	Maceió	−9.55	−35.77	84.12	1867.25	26.64
5	Natal	−5.84	−35.21	47.68	1616.26	25.82
6	Recife	−8.06	−34.96	11.3	2276.68	3.28
7	Salvador	−13.01	−38.51	47.35	1968.17	18.85
8	São Luís	−2.53	−44.21	32.58	2094.54	13.93
9	Teresina	−5.03	−42.80	75.73	1262.36	31.56

** Note: The percentage of faults is the count of faults existing at each station, which was filled in by the imputation method.

In this paper, we used the method proposed by Harrel [33] and Junger and Ponce de Leon [34] for missing data filling in the yeas. The percentages of missing data in the precipitation time series to the following criteria: (i) percentage ≤ 0.05 : single imputation is applied or only complete data are analyzed; (ii) percentage between 0.05 and 0.15: single imputation is used; and (iii) percentage greater than 0.15: multiple imputations are indicated in most cases [35,36]. After quality control and filling of gaps in the rainfall data, descriptive statistics were applied.

2.3. ENSO and PDO

To better understand the variability, the influence of ENSO was included, characterized by its phases: positive (El Niño), negative (La Niña), and neutral. The ENSO phases are classified according to the Sea Surface Temperature (SST) anomalies of the Equatorial Pacific

region, called the El Niño 3.4 region, via the Oceanic Niño Index (ONI) [37], according to Table 3. According to the link, information about the occurrences of ENSO phases is based on data from the National Weather Service (NWS) and the National Oceanographic and Atmospheric Administration (NOAA) (<https://ggweather.com/enso/oni.htm>, accessed on 8 August 2022).

Table 3. Occurrences of ENSO—Oceanic Niño Index (ONI). Source: The intensity of the categories is found on the website: <https://ggweather.com/enso/oni.htm>, accessed on 8 August 2022.

El Niño				La Niña		
Weak	Moderate	Strong	Very Strong	Weak	Moderate	Strong
1952–53	1951–52	1957–58	1982–83	1954–55	1955–56	1973–74
1953–54	1963–64	1965–66	1997–98	1964–65	1970–71	1975–76
1958–59	1968–69	1972–73	2015–16	1971–72	1995–96	1988–89
1969–70	1986–87	1987–88		1974–75	2011–12	1998–99
1976–77	1994–95	1991–92		1983–84	2020–21	1999–00
1977–78	2002–03			1984–85		2007–08
1979–80	2009–10			2000–01		2010–11
2004–05				2005–06		
2006–07				2008–09		
2014–15				2016–17		
2018–19				2017–18		

In addition, the influence of the PDO phases was also addressed, characterized by having two phases: (i) positive—hot (1925–1946; 1977–1998) and (ii) negative—cold (1947–1976). The temperature anomalies define the two phases in the Northeast and the Tropical Pacific Ocean through the NCDC Index (National Climatic Data Center)/USA: Based on “reconstructed” data from SST in the Pacific. Information about PDO occurrences is at the National Centers for Environmental Information (NCEI), according to the link: <https://www.ncdc.noaa.gov/teleconnections/pdo/>, accessed on 8 August 2022.

The variability of annual rainfall in the capitals of the NEB was based on the identification of dry and rainy years in the studied period associated with ENSO phases via the ONI index and the PDO phases via the NCEI PDO index. To facilitate the discussion of the results obtained in the study, the following criterion was adopted: North of the NEB (NNEB)—(MA, PI, CE, and RN), East of the NEB (ENEb)—(PB, PE, AL, and SE) and South of the NEB (SNEB)—(BA).

2.4. Mann–Kendall Test

To identify statistically significant trends in the time series of the assembled NEB precipitation dataset, the Mann–Kendall test (MK) [38] was applied. MK test can use the same time series distribution by enabling the stability of the hypothesis for successive and independent occurrences [38,39], using the below by Equation (1).

$$S = \sum_{j=i+1}^n \text{sgn}(x_j - x_i) \tag{1}$$

where x_j is the estimated date of the sequence of values, n is the length of the time series, and the sign S is given by Equation (2):

$$S = \begin{cases} \text{andsgn}(x) = 1 & \Leftrightarrow \text{for } (x_j - x_i) > 0 \\ \text{andsgn}(x) = 0 & \Leftrightarrow \text{for } (x_j - x_i) = 0 \\ \text{andsgn}(x) = -1 & \text{for } (x_j - x_i) < 0 \end{cases} \tag{2}$$

The values $(x_1, x_2, x_3, \dots, x_n)$ in time series with $(n > 4)$ terms assuming the null hypothesis (H_0) is defined by Equation (3).

$$Var(S) = \frac{n(n-1)(2n+5)}{18} \tag{3}$$

Furthermore, the variation can be find out by Equation (4):

$$Var(S) = \frac{1}{18} \left[n(n-1)(2n+5) - \sum_{p=1}^g t_p(t_p-1)(2t_p+5) \right] \tag{4}$$

where n , t_p and p_{th} is observations, observation after equal time and the data values in a given group p , respectively.

For the evaluation of the statistical significance of S for H_0 with a two-tailed test, it can be rejected for higher values of the MK statistic, which is defined by Equation (5):

$$Z_{MK} = \begin{cases} \text{and } \frac{S-1}{\sqrt{Var(S)}} \text{ for } S > 0 \\ \text{and } 0 \text{ for } S = 0 \\ \text{and } \frac{S+1}{\sqrt{Var(S)}} \text{ for } S < 0 \end{cases} \tag{5}$$

Based on Z_{MK} statistics, hypothesis H_0 can be positive with null trend (for p -value $> \alpha$) and is omitted for another hypothesis (H_1) for significant trend with p -value $< \alpha$. This study has been done with a confidence level of 5% (Table 4).

Table 4. The significant Z_{MK} values in the probability range from -1.96 to $+1.96$.

Category	Scale
Significant trend of increase (STI)	$Z_{MK} > +1.96$
Non-significant increasing trend (NSIT)	$Z_{MK} < +1.96$
No trend (NT)	$Z_{MK} = 0$
Non-significant downward trend (NSDT)	$Z_{MK} > -1.96$
Significant downward trend (SDT)	$Z_{MK} < -1.96$

In this paper, the methods are executed with Z statistic, where positive values ($Z > 0$) and negative values ($Z < 0$) show an increasing and decreasing trend, respectively.

3. Results and Discussion

3.1. Analysis of Rainfall in NEB Capitals

3.1.1. Annual

In descriptive statistics, Aracaju had the lowest annual average (1382.7 mm), while Recife (2276.7 mm) and São Luís (2094.5 mm) stand out with the highest averages in the time series. This difference is motivated by the performance of TWD and EWD in Recife, together with ITCZ and LI in São Luís, which contribute to the highest rainfall records, respectively [14,39]. Concerning the maximum values, the highlight goes to João Pessoa (3888.4 mm), Recife (3527.1 mm), Salvador (3223.2 mm), and, mainly, São Luís (3981.3 mm), with annual totals similar to those recorded in the Legal Amazon [3] (Table 5). The capital São Luís is surrounded by mangroves, sea, and rivers on all sides. It is located on the limits between the Caatinga vegetation and the Amazon Forest. It directly influences dry and humid air masses, with higher rainfall records compared to the other capitals of the NEB [40,41].

The minimum values obtained in the study were identified in the capitals of João Pessoa and Teresina, mainly in the latter (<340 mm) (Table 5), the only capital that is not located in a coastal environment (Figure 1) and is not varied by precipitation transmission and LI decrease significantly. The highest (lowest) values of standard deviation (SD) were verified in São Luís, João Pessoa, and Fortaleza (Natal and Teresina). The median’s highest

(lowest) value was obtained in the city of Recife (Aracaju). As for the values of coefficient of variation (CV %), all the capitals of the NEB present a strong dispersion of data, to which values were lower than 35%, highlighting the capitals with CV % lower than 25%; this demonstrates the regularity in the distribution of annual rainfall [35,36].

Table 5. Descriptive statistics applied to annual rainfall (mm) in NEB capitals.

Capitals	\bar{x} (mm)	m_d (mm)	SD (mm)	Max (mm)	Min (mm)	CV (%)
Aracaju	1382.7	1328.1	432.3	3126.3	738.0	31%
Fortaleza	1607.6	1620.8	513.9	2900.1	636.2	32%
João pessoa	1906.1	1971.5	637.8	3888.4	501.2	33%
Maceió	1867.3	1825.4	436.3	3033.1	997.2	23%
Natal	1616.3	1527.3	349.3	2485.9	849.0	22%
Recife	2276.7	2260.4	468.4	3527.1	1249.7	21%
Salvador	1968.2	1999.6	393.1	3223.2	1233.2	20%
São Luís	2094.5	1966.4	627.0	3981.3	647.0	30%
Teresina	1262.4	1267.0	296.1	2028.0	334.8	23%

(a) *East of the NEB (ENEB)*

In Aracaju, during the negative phase of the PDO (1947–1976) (Figure 2a), there were rainy years until the mid-1970s. However, in the subsequent cycle referring to the positive phase of the PDO (1977–1998), there was a significant decrease in its total rainfall, mainly from the second half of the 1990s. In the 2000s and 2010s, the PDO performance in the negative phase (1999–current days) contributed to years with below-average rainfall (1403 mm). According to Da Silva et al. [30], the PDO's performance intensifies the ENSO phases in the NEB. During the analyzed period, Aracaju had some rainy (dry) years, mainly between 1964 and 1968 (1961 to 1963 and 2004 to 2014). Among the years analyzed, 1983 (El Niño Strong) and 2016 (El Niño Very Strong) stand out with the lowest rainfall records [2,6,38], which recently have been called Mega-El Niño in the literature [42,43].

Regarding the years with higher-than-average rainfall, the biannual cycles 1964–1965 (La Niña Weak) and 1974–1975 (La Niña Strong) stand out, with the highest annual rainfall records. The records of rainy years is associated with ENSO phases in the NEB [3,6,7] and are even found in Aracaju [44].

The capital Maceió (Figure 2b) has high variability of annual rainfall; for example, in the 1960s and 1970s, with the highest records of annual rainfall (negative phase of the PDO), on the contrary, in the 1980s and 1990s, with lower annual rainfall records (positive phase of PDO). Recently, Oliveira-Júnior et al. [41] identified, based on CHELSA's precipitation product (Climatologies at High Resolution for the Earth's Land Surface Areas) In contrast, the decadal variability corresponded to the PDO phase shift, similar to the results obtained in the study. The highest annual rainfall records occurred in the 2000s, and the lowest annual rainfall was recorded in the 2010s, with PDO in the negative phase. Previously, Lyra et al. [5] related the wet and dry periods in Alagoas via Harmonic and Spectral Analysis (HSA) and identified patterns similar to those found in this study, but with a lower time series of data (1960–1990) and fewer stations (33 stations). When referring to the average of the driest years, in this case, 34 years, the total rainfall is lower than the average (1867.4 mm) in Maceió, but higher than the total obtained in Aracaju.

Highlighting the years 1998 (El Niño Very Strong) and 2020 (El Niño Weak), with the lowest rainfall records in Maceió, such results are previously corroborated by Oliveira Júnior et al. [45] and Lyra et al. [5], and recently by Costa et al. [7] and Oliveira Júnior et al. [46]. At the same time, in the 27 years that presented above-average rainfall, the years 2000 and 2009 (La Niña Weak) and 2017 (La Niña Strong) stand out.

The capital Recife (Figure 2c) shows a decrease in rainfall throughout the time series, except for the 1960s with the highest annual rainfall records, which remained until 1974 (negative PDO phase), similar to Aracaju and Maceió. Although 1977 to 1998 corresponds to the positive phase of the PDO, the rainfall totals between 1984 and 1990 were above

average (2276.7 mm). The 1990s (2000 and 2010) exhibited the driest years (alternating between wet and dry years). There is evidence of the role of the PDO in the rainfall regime on the ENEB coast concerning the hot (1977–1998) and cold (1947–1976) phases [5,8,10,11]. Regarding the 31 years with lower than average rainfall in Recife, the biannual cycles 1997–1998, 1982–1983, and 2015–2016 (El Niño Very Strong) stand out. Concerning the 30 years with above-average rainfall in Recife, 1964 (La Niña Weak), 2000, and 2011 (La Niña Strong) stand out. Such average rainfall is due to the action of meteorological systems, for example, TWD, EWD, and breeze circulations, followed by the continentally and maritime effects [16,17].

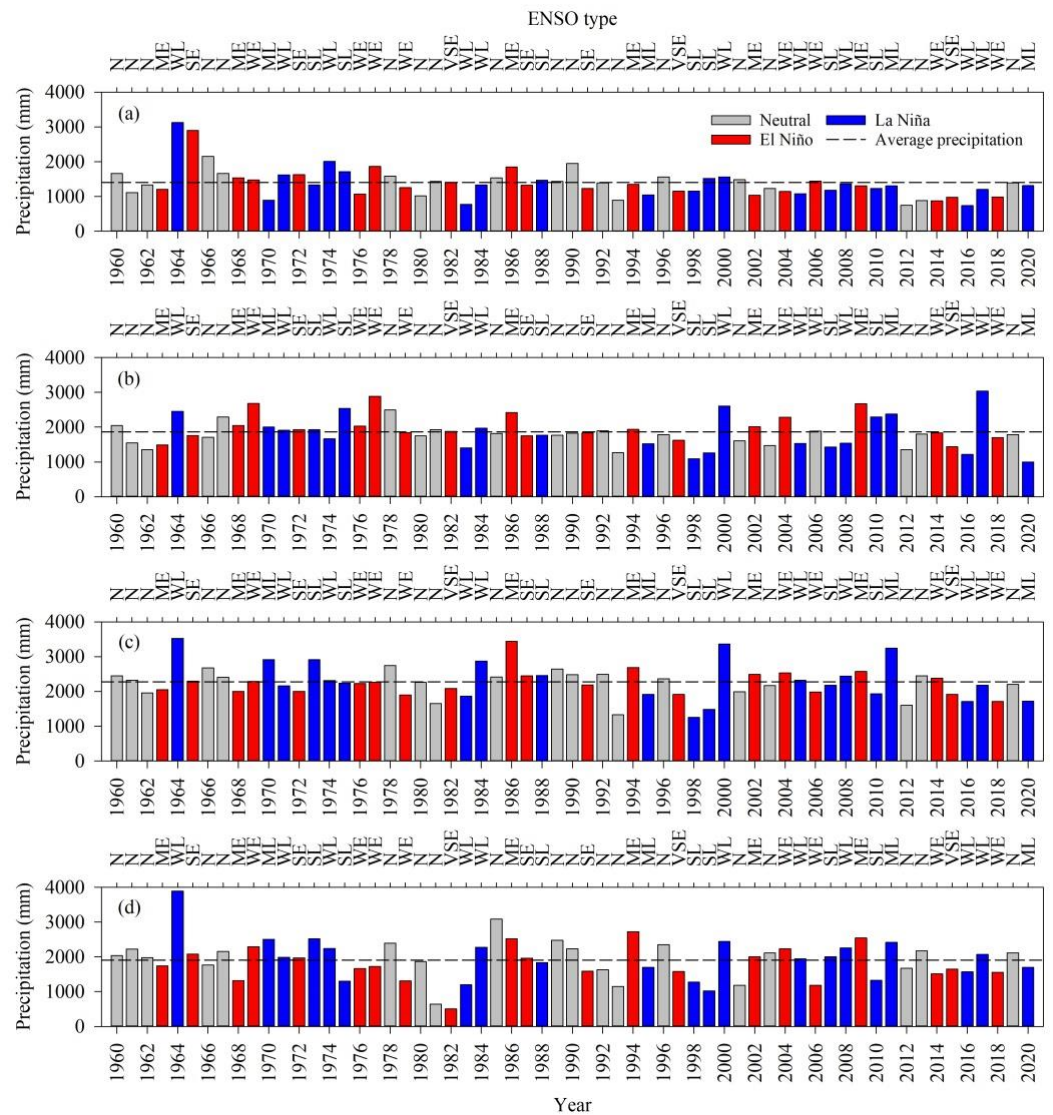


Figure 2. Annual rainfall distribution (mm/year) in ENEB capitals—Aracaju (a), Maceió (b), Recife (c), and João Pessoa (d). El Niño, La Niña, Neutral, and their intensities based on the Oceanic Niño Index (ONI): N: Neutral, WE: weak El Niño; ME: moderate El Niño; SE: strong El Niño; VSE: very strong El Niño; WL: weak La Niña; ML: moderate La Niña; and SL: strong La Niña. The colors in the bars are Neutral in grey, La Niña in blue, and El Niño in red, and the dashed line represents average rainfall for the period 1960–2020.

The capital João Pessoa (Figure 2d) has high rainfall variability compared to other ENEB capitals, until the mid-1970s, when the rainiest years were recorded (negative phase of the 1949–1976 PDO). From the second half of the year onwards from the 1970s to the 1990s, drier years were recorded (positive phase of the PDO) [47]. Regarding the 28 years

with lower (higher) rainfall than the average of 1.906 mm, the 1982–1983 biannual cycle (1964, 1985, and 2009) resulting from the Very Strong El Niño (La Niña Weak) stands out, with the lowest (highest) annual rainfall record.

(b) North of the NEB (NNEB)

In São Luís (Figure 3a), it can be seen that the negative phase of the PDO (1947–1976), the 1960s, was characterized by annual rainfall below average (2094.5 mm). From the 1970s onwards, there were some years with annual rainfall above the average, for example, between 1970–1975, except 1972. It is noted that during the positive phase of the PDO (1977–1998), the annual rainfall pattern shows strong variability. As for the period analyzed, the years 1971, 1984–1985 (La Niña Weak), and 1973–1974 (La Niña Strong) stand out, with the highest annual rainfall records influenced by the performance of the ENSO [48].

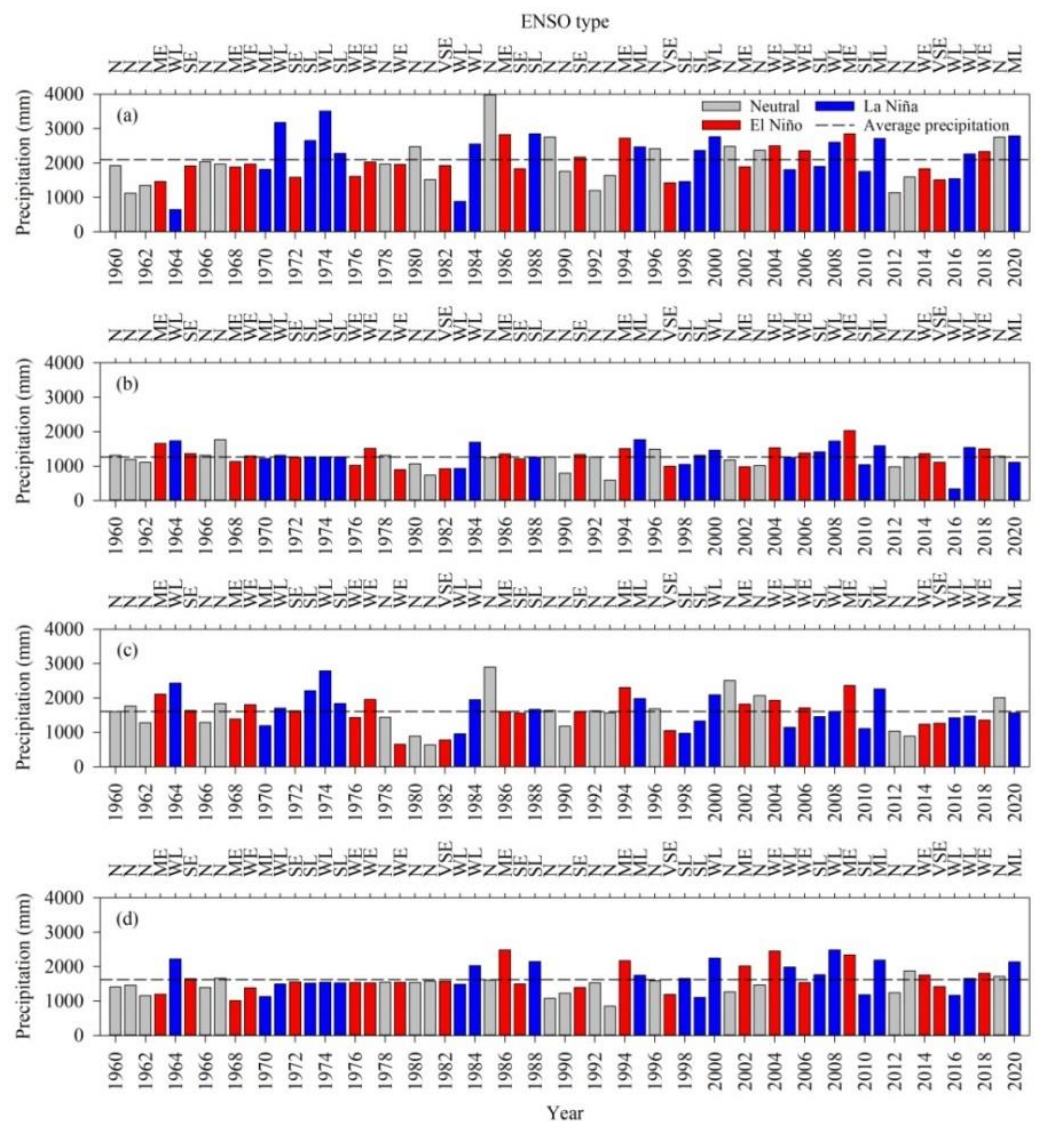


Figure 3. Annual rainfall distribution (mm/year) in the capitals of the NNEB—São Luís (a), Teresina (b), Fortaleza (c), and Natal (d). El Niño, La Niña, Neutral, and their intensities based on the Oceanic Niño Index (ONI): N: Neutral, WE: weak El Niño; ME: moderate El Niño; SE: strong El Niño; VSE: very strong El Niño; WL: weak La Niña; ML: moderate La Niña; and SL: strong La Niña. The colors in the bars are Neutral in grey, La Niña in blue, and El Niño in red, and the dashed line represents average rainfall for the period 1960–2020.

The capital Teresina (Figure 3b) is the only capital of the NEB far from the coast; in addition, it is the only one that has a significant decrease in annual rainfall when compared to the other capitals of the NNEB, as it is a region marked by low air humidity and high temperatures [10]. In the 1960s, some years had higher or close to average rainfall until 1976 (negative PDO phase). The period from 1977 to 1998 presents high variability of annual rainfall, verified mainly in the 1980s, with several years with below-average rainfall, except for 1984, corresponding to the positive phase of the PDO. In the cold phase of the PDO (1999–current days), the 2000s show high rainfall records, the opposite of the low records in the 2010s.

The capital Fortaleza (Figure 3c) shows a decrease in rainfall over the decades. Between the years 1960 and 1975 (1976 and 1998), it appears that the high (low) rainfall records occurred during the negative phase of the PDO (negative phase of the PDO), mainly in the 2000s (2010s), were the wettest (dry), with a total of 17,689.6 mm (14,503.28 mm). Silva et al. [21] found that the association of ENSO and PDO in the same phase promotes a decrease (increase) in annual rainfall totals during the hot (cold) phase of both events. Of the 31 years with lower than average rainfall (1607.6 mm) in Fortaleza, the years 1979 (El Niño Weak) and 1982 (El Niño Very Strong) stand out, with the lowest annual rainfall records. Meanwhile, of the 29 years that had higher than average rainfall in Fortaleza, the biannual cycle of 1973–1974 and 2011 stands out, resulting from the performance of La Niña Forte. Severe droughts in the NEB have been linked to the occurrence of El Niño. The relationship between El Niño and droughts in the NEB is ambiguous because of the 46 El Niños (strong and moderate) from 1849–1992; 21 (45%) were associated with severe droughts in Fortaleza.

The capital Natal (Figure 3d) shows an increase in rainfall over recent decades. Despite being under the negative phase of the PDO, the 1960s had the lowest annual rainfall records. The 1970s, 1980s, and 1990s had the highest rainfall records below average (positive phase of the PDO). Corresponding to the negative phase of the PDO, the 2000s had the highest annual rainfall records, and the 2010s had high rainfall records in most years.

Of the 38 years with below-average rainfall (1616.3 mm), the years 1968 (El Niño Moderate) stand out, with the lowest annual record of rain, while the 23 years with above-average rainfall in Natal stand out in the years 2008 (La Niña Strong) and 2009 (La Niña Weak). According to Silva et al. [21], through SPI and Wavelet, the simultaneous interactions of different time scales explain high rainfall values for Natal and the influences of ENSO, GIASST, Sunspots, and PDO.

(c) *South of the NEB (SNEB)*

In relation to SNEB cities, Salvador (Figure 4) shows a significant decrease in rainfall from 1978 onwards. The decade from 1960 to 1975 stands out, with the wettest year corresponding to the negative phase of the PDO. Then, the capital went through a cycle of below-average rainfall (1977–1998), corresponding to the positive phase of the PDO [30,49]. In this next negative phase of the PDO, the 2000s had slightly higher rainfall records than the previous decade, and the 2010s had the least rainfall (17,187 mm).

Of the 30 years with lower than average rainfall (1968.17 mm), the year 2016 (El Niño Very Strong) stands out with the lowest annual record of rainfall, while the 31 years with higher than average rainfall stand out the years 1964 (La Niña Weak) and 1999 (La Niña Strong). SNEB shows a strong relationship between rainfall variability and ENSO phases [49]. The percentages identified show rainfall variability as a function of ENSO phases. However, the human influence on rainfall dynamics cannot be ruled out, particularly the urbanization process that has altered rainfall patterns in Brazil and the NEB [19,50].

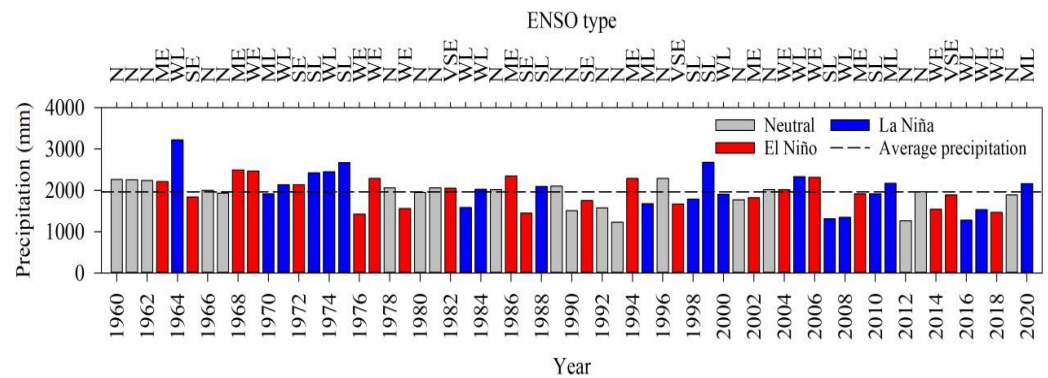


Figure 4. Annual rainfall distribution (mm/year) in the SNEB capital—Salvador. El Niño, La Niña, Neutral, and their intensities based on the Oceanic Niño Index (ONI): N: Neutral, WE: weak El Niño; ME: moderate El Niño; SE: strong El Niño; VSE: very strong El Niño; WL: weak La Niña; ML: moderate La Niña; and SL: strong La Niña. The colors in the bars are Neutral in grey, La Niña in blue, and El Niño in red, and the dashed line represents average rainfall for the period 1960–2020.

Figure 5 shows the occurrence of ENSO events in the NEB capitals. The percentages identified show rainfall variability as a function of ENSO phases. However, the human influence on rainfall dynamics cannot be ruled out, particularly the urbanization process which has altered rainfall patterns in Brazil and the NEB [19,50]. During the evaluated period (1960 to 2020), there were several occurrences of ENSO in the Neutral phase. On the other hand, the presence of weak El Niño (WE) and weak La Niña (WL) justify the variability of rainfall in all capita areas of the NEB. These oscillations in weak, moderate, or severe phases can cause variations in the volumes and the beginning of the rainy seasons.

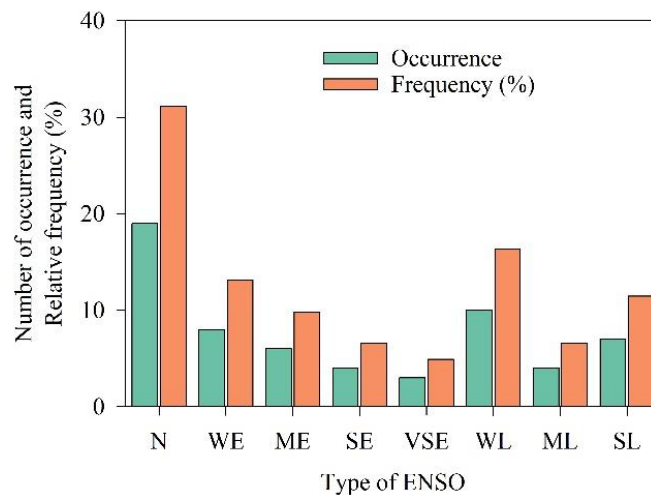


Figure 5. The occurrence of ENSO intensities in NEB capitals from 1960 to 2020. Note: Neutral (N), weak El Niño (WE), moderate El Niño (ME), strong El Niño (SE), very strong El Niño (VSE), weak La Niña (WL), moderate La Niña (ML), and strong La Niña (SL).

3.1.2. Seasonal

Figure 6 shows the boxplot of the average monthly rainfall in ENEB during the study period. In Aracaju (Figure 6a), the highest (lowest) median value occurs in May (December), with a value of 279.1 mm (26.4 mm). The highest (lowest) interquartile range (IQR) occurs in May (August), with a value of 218.1 mm (35.4 mm). The months between January and June showed greater dispersion of rainfall data, with a larger occurrence of outliers, due to the influence, mainly, of the ITCZ, which occurs between March and April, followed by February and May [10,17]. On the other hand, with the absence of the ITCZ, the capital and the state of Sergipe has frequent rainfall reductions, especially in the semi-arid region [44].

The influence of the rest of FS, TWD, EWD, and breezes circulation [10]. This dispersion decreased significantly in July, October, November, and December, with fewer outliers and a decrease in rainfall-producing systems [48,49].

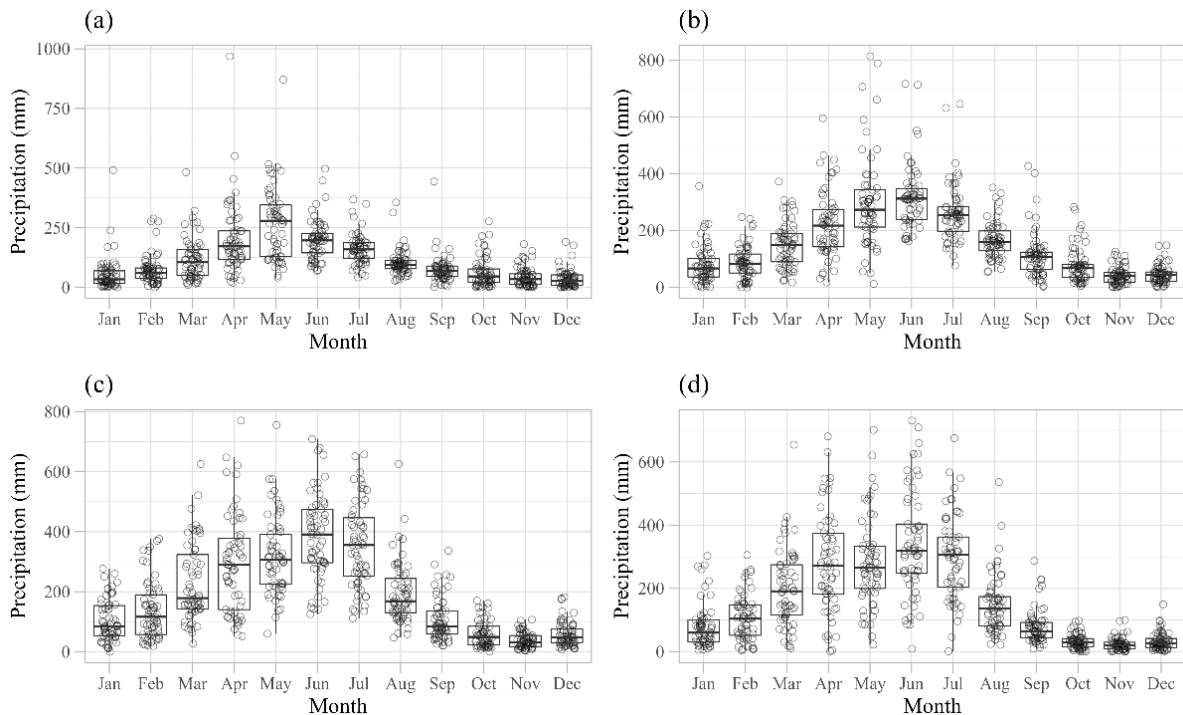


Figure 6. Monthly rainfall boxplot (mm) at ENEB—Aracaju (a), Maceió (b), Recife (c), and João Pessoa (d) from 1960 to 2020.

In Maceió (Figure 6b), the highest (lowest) median occurred in June (November) with a value of 312.3 mm (40.6 mm), as well as the lowest IQR (36.2 mm); on the contrary, in May (136.3 mm). Between April and July, there was a greater dispersion of data (outliers); on the contrary, in the period between August and December, with a decrease in this dispersion. The seasonality of rainfall in Maceió is due to the action of multiscale meteorological systems, for example, HLCV, SASH, EWD, TWD, and the circulation of sea/land and lagoon breezes [5,7,30,46]. Furthermore, the influence of the urbanization process and changes in land use and occupation cannot be ruled out, particularly since the 1990s, as recently identified by Correia Filho et al. [3] and Oliveira Júnior et al. [45].

The results observed for Recife (Figure 6c) followed the same pattern as for Maceió, with the highest (lowest) median in June (November) with a value of 390.8 mm (31.3 mm), with greater dispersion between March and July, due to EWD and less dispersed data between September and December, when the lowest rainfall records occur (Ferreira, 2016). Likewise, João Pessoa (Figure 6d) had the highest median in June (318.8 mm) and the lowest in November (29.9 mm). From March to August, there was greater dispersion of data, with a significant decrease from October to December. In both capitals, April was the month with the highest IQR (244.0 mm and 201.9 mm), and November had the lowest (37.8 mm and 20.6 mm).

The ENEB has particular climatic characteristics, as the NEB is in the tropical belt location of South America. This sub-region is under the influence of several meteorological systems, in addition to the proximity to the Equator and, thus, a greater amount of solar radiation [44]. The ITCZ occurs from March to April, and the penetration of cold air from polar air masses is normally associated with the formation of SF, which influences the dynamics of rain between April and August [5,12]. On the other hand, the EWD that occurs between May and July is mainly responsible for the occurrence of rain in the period and,

finally, the circulation of breezes that affect the rainfall regime on the coast, with greater intensity in the period from May to June [1,11].

The rainfall caused by the HLCV in the ENEB depends on its position, as upward air movements are observed on the western and northern edges, which can cause flooding. In contrast, in the center of the vortex, subsidence movements cause stable weather in the region below [7,9]. They also showed that the SASH contributes to rainfall on the ENEB coast when it is located further south of its average position and is close to the coast of SA. Positive SST anomalies in the South Tropical Atlantic produce rain over the ENEB. In contrast, positive SST anomalies in the Pacific inhibit rainfall [1]. Therefore, seasonal rainfall in ENEB is influenced by the following systems: ITCZ, FS, EWD, TWD, circulation of breezes, HLCV, and SASH [5,12].

Figure 7 shows the boxplot of the average monthly rainfall in the NNEB during the study period. In the capital São Luís (Figure 7a), the highest (lowest) median occurred in April (October) with a value of 429.3 mm (1.0 mm), highlighting this month with the lowest median among the NEB capitals. The months of February, April, and May had the greatest dispersion of data (outliers), corresponding to the months of greater activity of the ITCZ and the rainy season in the region [10], while the period of August and November had less dispersion, corresponding to the dry period of the region. January (October) had the highest (lowest) IQR with a value of 223.3 mm (5.2 mm). The main rainfall mechanism in São Luís is the ITCZ [10], followed by LI's and breeze circulations [8,50–53]. Previous studies also reported these analyses using ground and space-based measurement data [48–52].

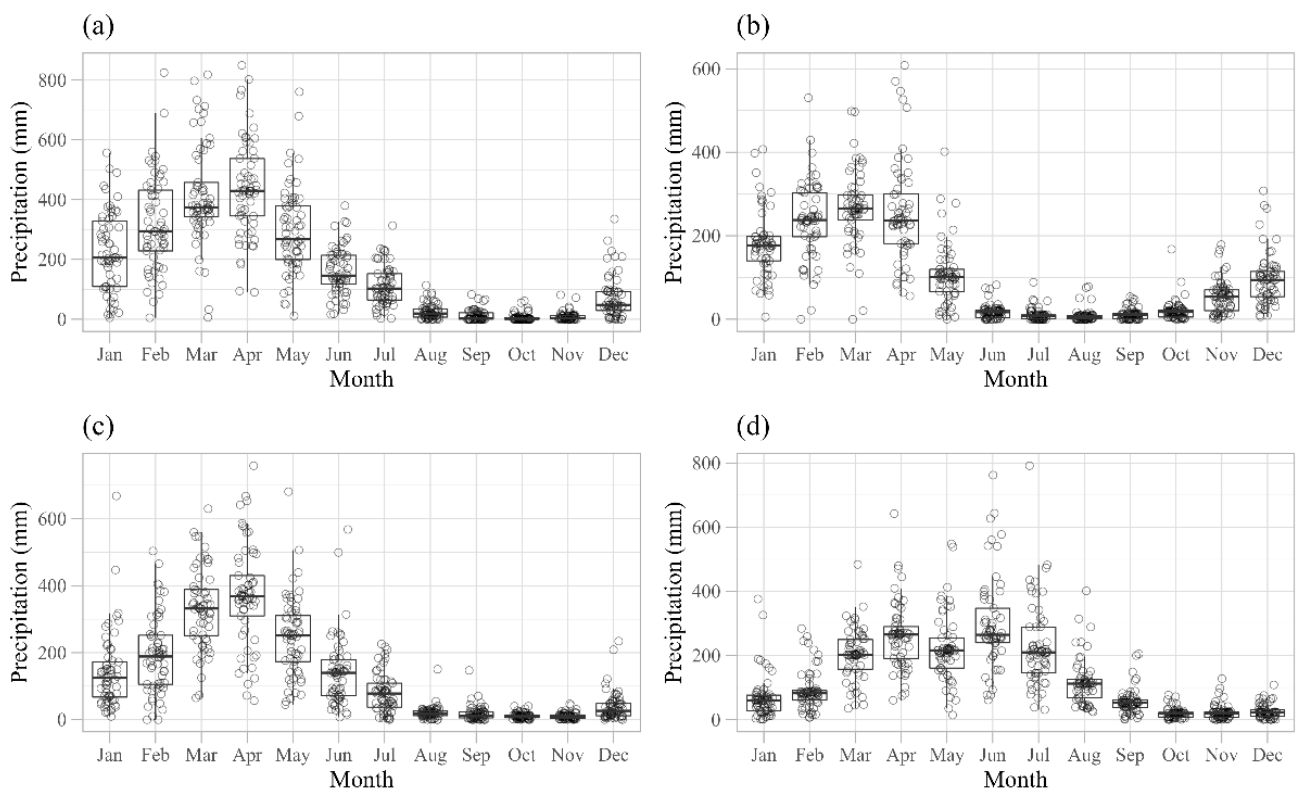


Figure 7. Monthly rainfall boxplot (mm) in NNEB—São Luís (a), Teresina (b), Fortaleza (c), and Natal (d) in the period from 1960 to 2020.

In Teresina (Figure 7b), the highest (lowest) median occurred in March (August), with a value of 264.3 mm (5.4 mm), as well as the lowest value of IQR (8.0 mm). Between December and May, there was greater dispersion of data, with a significant decrease between June and November. Moreover, April had the highest IQR (124.8 mm). Fortaleza (Figure 7c) had the lowest (highest) median, which occurred in November (April), with a value of 9.5 mm (368.2 mm). Between December and June, there was greater dispersion of data, with a

significant decrease between August and November. The highest IQR occurred in May, and the lowest was in October. The capital Natal (Figure 7d) followed the same pattern as São Luís, with the highest median in April (265.2 mm) and the lowest in October (18.4 mm), as well as the lowest IQR (14.4 mm) and the highest IQR, which occurred in July (143.4 mm). There was greater dispersion of data between January and August, decreasing significantly in October, November, and December.

The NNEB is characterized by a rainy period (between February and May) with high inter-annual variability [54–56] and no rain during most of the dry period (October–December). The influence of El Niño is marked on the NNEB, and there is a high probability of droughts, associated, in 70% of cases, with moderate to severe episodes. La Niña events have been associated with wetter than normal rainy seasons. In the NNEB, the meteorological systems operate on a synoptic scale: ITCZ, HLCV, EWD, SACZ, and FS; in mesoscale: LI and SCMs; and on a local scale: isolated storms and breeze circulations [14,53]. The most probable results also provided deep insights in previous reports [57–62].

Figure 8 shows the boxplot of the average monthly rainfall in the SNEB during the study period. In Salvador, the highest median occurred in May (323.6 mm), with the Atlantic Dipole mode being one of the main rain inducers since it influences the positioning of the ITCZ. The lowest occurred in January (85.9 mm); in this period, HLCV penetrates the interior of the NEB, causing clear skies in the SNEB [57,63–66]. The months of January, July, and August (September to December) were the months with the highest (least) data dispersion (outliers). April (August) is the month with the highest (lowest) IQR, with a value of 188.3 mm (47.4 mm).

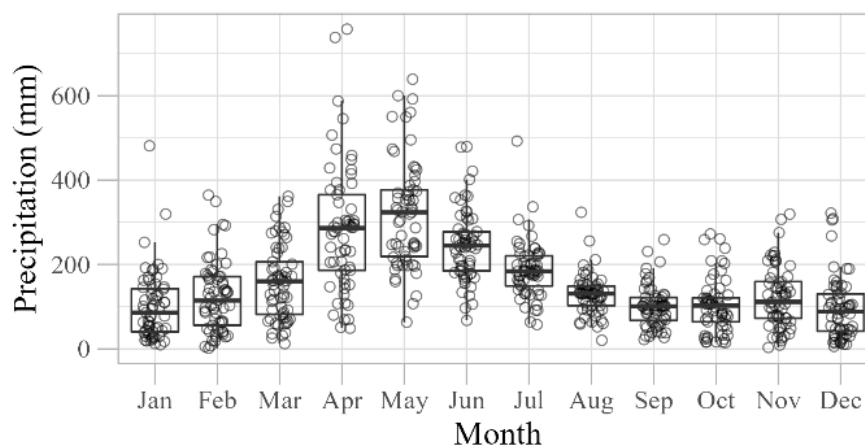


Figure 8. Monthly rainfall boxplot (mm) in SNEB—Salvador from 1960 to 2020.

The FS, an important rain-producing system, acts basically in the SNEB, from November to February, with the maximum recorded in December, mainly in the southern part of Bahia, and decreasing towards the north of the region. The SNEB has high monthly rainfall totals throughout the year, but the highest volumes occur from April to July. Several atmospheric systems act on the NEB and affect, directly or indirectly, the rainfall regime of Salvador; they are ITCZ, SASH, SACZ, EWD, TWD, FS, HLCV, and MCC. In addition, Salvador is influenced by the sea breeze system on its Atlantic coast, which acts as a thermal regulator for the city, mitigating the high temperatures from September to February [1,8].

3.2. Rainfall Trend in NEB Capitals

In all the evaluated NEB capitals, there was no anomalous variations in annual rainfall ($Z_{MK} > +1.96$)—only a low growth ($Z_{MK} < +1.96$) in rainfall, similar to the results obtained by Oliveira-Júnior et al. [40]. This result is worrying in terms of water supply, supply of reservoirs, and especially for urban agriculture, as 12,602,080 inhabitants live in the capitals (Table 1) [32]. Note the absence of trend ($Z_{MK} = 0$) in all capitals of the NEB (Table 6).

Table 6. Rainfall trend via MK test applied to Northeast capitals.

Capitals	Z _{MK} Values
Aracaju	−4.24
Fortaleza	−1.43
João Pessoa	−1.32
Maceió	−2.22
Natal	−1.01
Recife	−1.44
Salvador	−4.64
São Luís	−0.29
Teresina	−1.14

Detecting anomalous pattern from stations data of rainfall is of intense care [34], especially in Brazil, which depends on various agri-business processes with enormous populated regime on the coast [40,43].

Individually, the capitals that showed decrease rainfall ($Z_{MK} > -1.96$) were Fortaleza, João Pessoa, Natal, Recife, São Luís, and Teresina. Both capitals showed significant rainfall deviation [8,12] as a result of ENSO and PDO processes [10] and, mainly, from GIASST [11].

On the other hand, the significant trend of decreasing rainfall in Aracaju, Maceió, and Salvador, corresponding to the share of ENEB and SNEB. Again, these cities decrease in the Sea shores Tablelands region [8]. The rise in land use by excessive urbanization during the 60 years in the above counties cannot be ruled out [25–27].

Previously, Silva [64] analyzed the climate variability of the NEB and detected significantly decreasing trends in several locations in the NEB region via the MK test. The author suggested in his study that this variability may be related to the occurrence of climatic changes in the NEB, from the semi-arid to the coastal area of the region, similar to the results obtained in the study, only for capitals of the NEB that are located on the coast, except for Teresina (Figure 1).

3.3. Relationship between Population and Average Rainfall

Figure 9 shows the comparative analysis of average rainfall annually and decennial urbanization during 1970–2020 in NEB capitals. The capitals of Aracaju (Figure 9a), Maceió (Figure 9d), João Pessoa (Figure 9c), Recife (Figure 9f), and Teresina (Figure 9i) showed a decreasing pattern in the decades 1980, 1990, and 2010 with respect to urbanization and rainfall relationship. At the same time, the capitals of Fortaleza (Figure 9b), Natal (Figure 9e), Salvador (Figure 9g), and São Luís (Figure 9h) showed an increasing trend, especially in the 2000s.

The disorderly occupation of cities causes changes in their physical characteristics. It makes the urban environment vulnerable to socio-environmental disasters like landslides and floods. On the other hand, urban expansion challenges water resource management, causing precipitation variations and generating problems in the water supply system [40,65,66].

In 1900, only 13% of the population lived in urban areas. In 2007, the urban population grew to 49.4% and thus occupied only 2.8% of the global territory. By 2050, it is estimated to be at 69.6% of the population in urban areas. In this context, the Brazilian population has grown [31] from 90 million to 205 million since 1970, and the urban population has increased from 55% to 84% [22]. The scenario is worrying since, historically, the greatest water deficits in Brazil have been recorded in the semi-arid region of the NEB, which is cyclically subjected to droughts and prolonged drought periods [3,55].

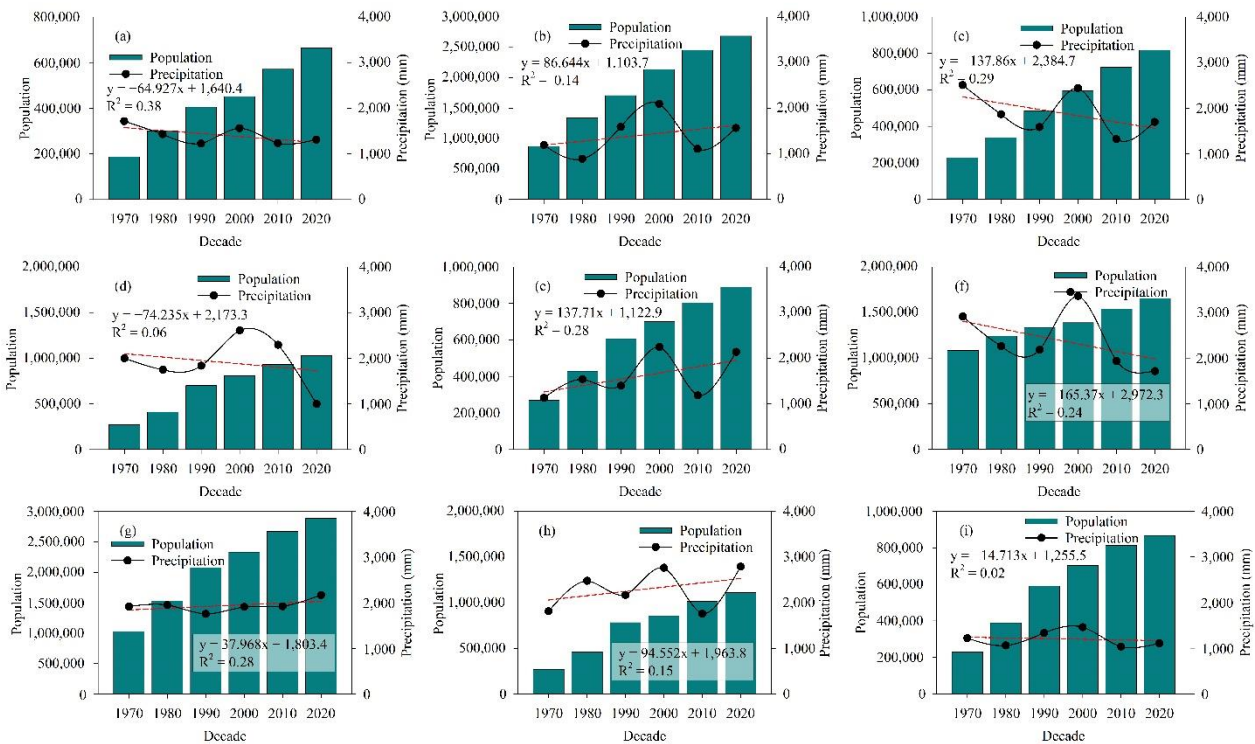


Figure 9. Relational pattern between average rainfall (mm) by decade and population (inhabitants) in the capitals of the NEB: Aracaju (a), Fortaleza (b), João Pessoa (c), Maceió (d), Natal (e), Recife (f), Salvador (g), São Luís (h), and Teresina (i).

3.4. Relationship between Climatological Normal and Observed Rainfall

Figure 10 shows the comparison between the observed rainfall and the climatological normal in the capitals of the NEB in the periods of 1961–1990, 1981–1990, and 1991–2020. Aracaju (Figure 10a) (−16%, 2%, and 11%) and São Luís (Figure 10h) (−6%, 5%, and 11%) show a significant decrease in the percentage of rainfall in the period 1961–1990 and an increase in the following two periods. Fortaleza (Figure 10b) (−31%, −35%, and 0.4%), Maceió (Figure 10d) (−11%, −4%, and 6%), Natal (Figure 10e) (−8%, −17%, and 3%) and Salvador (Figure 10g) (−14%, −1% and 5%), on the contrary, along with Aracaju and São Luís, showed a significant decrease in the percentage of rainfall in the periods 1961–1990 and 1981–1990, and an increase in the period 1991–2020. These statistical analyses provide more interesting information about NEB, like previous reports [67–71]. These methods also provided new insights into estimating rainfall measurements [72–76].

The highlight is that for João Pessoa (Figure 10c) (−8%, −11%, and −4%) and Teresina (Figure 10i) (−16%, −11%, and −8%), with a percentage decrease in rainfall in all the periods evaluated, such variations in accumulated rainfall will compromise the water supply [40,44]. On the other hand, Recife presented lower percentages of variation (1%, −2%, 6%), with a percentage decrease in rainfall only in the period 1981–1990 (Figure 10f) [56]. These long-term studies with different satellite data were also performed for different regions [72–76]. This study pointed out the variability of multiscale urban rainfall in the form of annual and seasonal variations in the capitals of the NEB. However, more analyses are needed with other satellite data to clear the phenomenon, like previous reports [77–81], which may provide more information on producing and inhibiting meteorological systems of rain in the NEB.

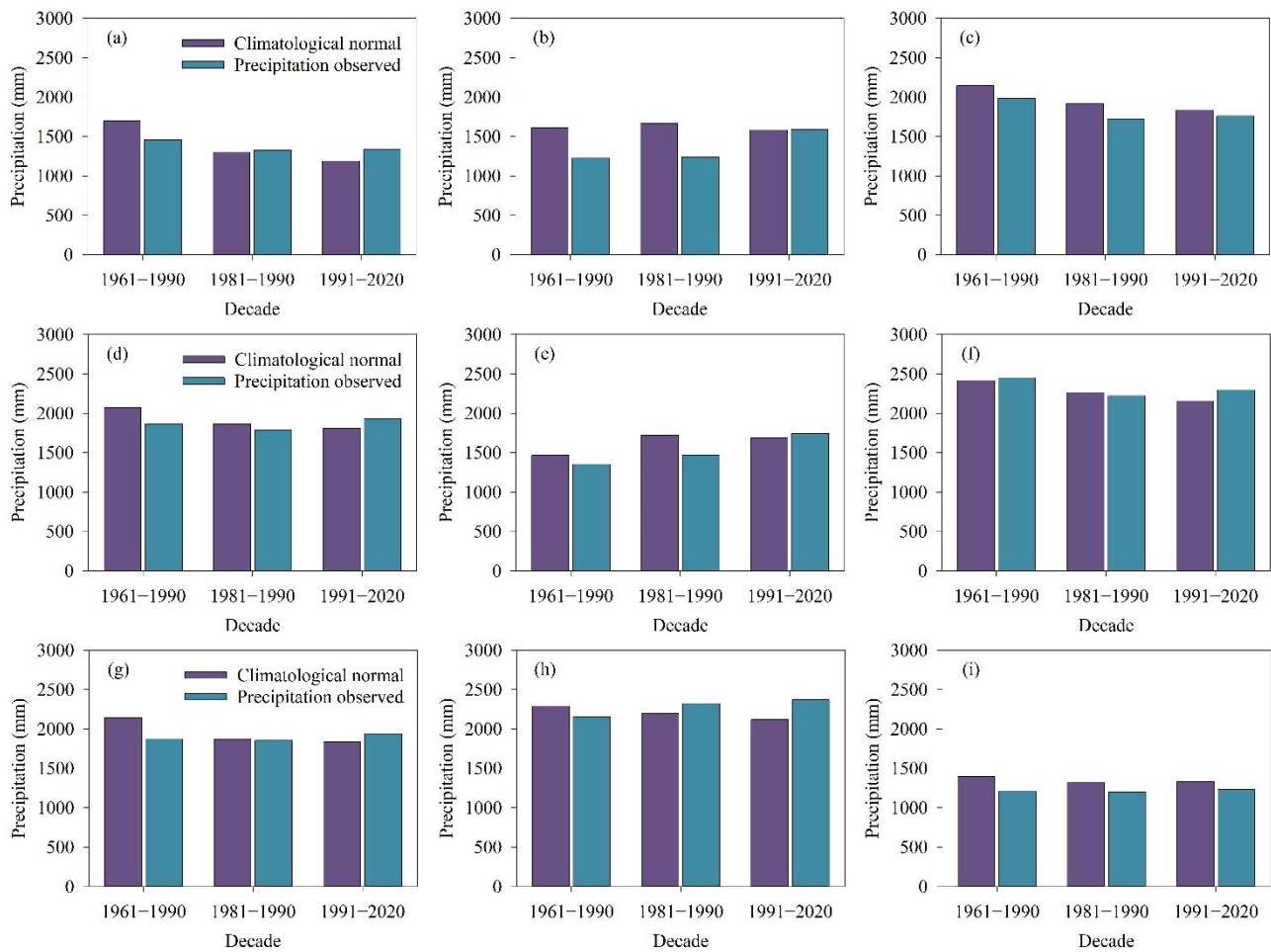


Figure 10. Comparison between observed rainfall and climatological normal in the capitals Aracaju (a), Fortaleza (b), João Pessoa (c), Maceió (d), Natal (e), Recife (f), Salvador (g), São Luís (h), and Teresina (i).

4. Conclusions

This study pointed out that the variability of multiscale urban rainfall (annual and seasonal) in the capitals of the NEB is directly associated with the ENSO phases, which may or may not be intensified according to the PDO phase, with a direct influence on producing and inhibiting meteorological systems of rain in the NEB. The anthropic influence cannot be ruled out, as there is a relational pattern of population growth and the variability of decennial rainfall in the capitals of the NEB, verified by the climatological normal. This change is possibly associated with the urbanization process that drastically influences the urban rainfall regimes in the study period, for example, changes in meteorological stations and urban densification in the observation sites.

The meteorological systems responsible for urban rainfall seasonality in ENEB are the ITCZ, FS, TWD, EWD, the breeze circulations, the HLCV, and the SASH. In the NNEB, the main meteorological systems operating are the ITCZ, HLCV, EWD, TWD, SACZ, SF, the LI, and the breeze circulations. Moreover, finally, in SNEB, the main systems are stationary FS, SACZ, local convection, and breeze circulations.

No capital of the NEB showed a significant trend of increasing annual rainfall. However, the cities of Aracaju, Maceió, and Salvador showed a significant trend of decreasing rainfall. The increase in population in the last decades in the capitals of the NEB and the notable decreasing trend of rain is worrying, as they will have problems with water supply.

The identification of the meteorological systems responsible for the occurrence of the seasonality of urban rainfall and its trend in the capitals of the NEB are points of

discussion of how changes in rainfall patterns in the capitals can lead to water shortages shortly, where periods of drought prolonged periods may compromise urban agriculture, which is remarkable in the NEB, mainly in terms of reducing investments in the industrial and tourist sectors, worsening the quality of life, and significantly increasing the region's social vulnerability. This is extremely important for developing new public policies and geo-environmental management for the capitals of the NEB.

Author Contributions: Conceptualization, J.F.d.O.-J. and L.d.S.M.; methodology, software, validation, L.d.S.M., J.F.d.O.-J., B.G. and W.L.F.C.F.; formal analysis, investigation, resources, M.S., S.Q., A.M.d.R.F.J., M.V.d.S., A.T. and A.K.; writing—original draft preparation, L.d.S.M., S.Q., F.M., A.T., M.A. and J.F.d.O.-J.; writing—review and editing, D.d.B.S., S.Q., H.G.B., D.M., M.C.A., A.d.S., L.C.G.P., J.L.B.d.S., A.K., A.T., S.Q., F.M. and M.A.; visualization, L.d.S.M., S.Q. and A.T.; supervision, A.T.; Funding, S.Q. All authors have read and agreed to the published version of the manuscript.

Funding: The research is financially supported by the National Natural Science Foundation of China Youth Fund (52209068), Postdoctoral Research Foundation of China (2020M682477), and the Fundamental Research Funds for the Central Universities (2042021kf0053).

Institutional Review Board Statement: Not applicable.

Informed Consent Statement: Not applicable.

Data Availability Statement: The data presented in this study are available on request from the first author.

Acknowledgments: The second author would like to thank the research productivity grant from the Conselho Nacional de Desenvolvimento Científico e Tecnológico (CNPq) level 2 under process number 309681/2019–7. The Coordenação de Aperfeiçoamento de Pessoal de Nível Superior (CAPES; Finance Code 001) and the Fundação de Amparo a Ciência e Tecnologia do Estado de Pernambuco (FACEPE) for the graduate scholarships.

Conflicts of Interest: The authors declare no conflict of interest.

References

1. Ullah, I.; Aslam, B.; Shah, S.H.I.A.; Tariq, A.; Qin, S.; Majeed, M.; Havenith, H.-B. An Integrated Approach of Machine Learning, Remote Sensing, and GIS Data for the Landslide Susceptibility Mapping. *Land* **2022**, *11*, 1265. [\[CrossRef\]](#)
2. Khalil, U.; Imtiaz, I.; Aslam, B.; Ullah, I.; Tariq, A.; Qin, S. Comparative analysis of machine learning and multi-criteria decision making techniques for landslide susceptibility mapping of Muzaffarabad district. *Front. Environ. Sci.* **2022**, *10*, 1–19. [\[CrossRef\]](#)
3. Sharifi, A.; Mahdipour, H.; Moradi, E.; Tariq, A. Agricultural Field Extraction with Deep Learning Algorithm and Satellite Imagery. *J. Indian Soc. Remote Sens.* **2022**, *50*, 417–423. [\[CrossRef\]](#)
4. Bera, D.; Das Chatterjee, N.; Mumtaz, F.; Dinda, S.; Ghosh, S.; Zhao, N.; Bera, S.; Tariq, A. Integrated Influencing Mechanism of Potential Drivers on Seasonal Variability of LST in Kolkata Municipal Corporation, India. *Land* **2022**, *11*, 1461. [\[CrossRef\]](#)
5. Fu, C.; Cheng, L.; Qin, S.; Tariq, A.; Liu, P.; Zou, K.; Chang, L. Timely Plastic-Mulched Cropland Extraction Method from Complex Mixed Surfaces in Arid Regions. *Remote Sens.* **2022**, *14*, 4051. [\[CrossRef\]](#)
6. Majeed, M.; Lu, L.; Haq, S.M.; Waheed, M.; Sahito, H.A.; Fatima, S.; Aziz, R.; Bussmann, R.W.; Tariq, A.; Ullah, I.; et al. Spatiotemporal Distribution Patterns of Climbers along an Abiotic Gradient in Jhelum District, Punjab, Pakistan. *Forests* **2022**, *13*, 1244. [\[CrossRef\]](#)
7. Costa, M.S.; Oliveira Júnior, J.F.; Santos, P.J.; Correia Filho, W.L.F.; Gois, G.; Blanco, C.J.C.; Teodoro, P.O.E.; Silva Junior, C.A.; Santiago, D.B.; Souza, E.O.; et al. Rainfall extremes and drought in Northeast Brazil and its relationship with El Niño-Southern Oscillation. *Int. J. Climatol.* **2021**, *41*, E2111–E2135. [\[CrossRef\]](#)
8. Molion, L.C.B.; Bernardo, S.O. Uma Revisão da Dinâmica das Chuvas no Nordeste Brasileiro. *Rev. Bras. De Meteorol.* **2002**, *17*, 1–10.
9. Costa, M.D.S.; Levit, V.; Federova, N. Padrões de circulação atmosférica no nordeste Brasileiro dos eventos de Vórtice Ciclônico de altos Níveis com Corrente de Jato. *Rev. Bras. Geo. Fis.* **2013**, *6*, 794–804. [\[CrossRef\]](#)
10. Reboita, M.S.; Gan, M.A.; Rocha, R.P.; Ambrizzi, T. Regimes de precipitação na América do Sul: Uma revisão bibliográfica. *Rev. Bras. Meteorol.* **2010**, *25*, 185–204. [\[CrossRef\]](#)
11. Lyra, G.B.; Oliveira Júnior, J.F.; Zeri, M. Cluster analysis applied to the spatial and temporal variability of monthly rainfall in Alagoas state, Northeast of Brazil. *Int. J. Climatol.* **2014**, *34*, 3546–3558. [\[CrossRef\]](#)
12. Hounsou-Gbo, G.A.; Servain, J.; Araújo, M.; Martins, E.S.; Bourles, B.; Canaix, G. Oceanic Indices for Forecasting Seasonal Rainfall over the Northern Part of Brazilian Northeast. *Am. J. Clim. Change* **2016**, *5*, 261–274. [\[CrossRef\]](#)

13. Costa, R.L.; Souza, E.P.D.; Silva, F.D.D.S. Aplicação de uma teoria termodinâmica no estudo de um Vórtice Ciclônico de Altos níveis sobre o Nordeste do Brasil. *Rev. Bras. Meteorol.* **2014**, *29*, 96–104. [CrossRef]
14. Silva, E.B.; Raposo, J.C.S.; Oliveira Júnior, J.F.; Correia Filho, W.L.F.; Santiago, D.B. Diagnóstico dos Casos de Dengue nas Capitais do Nordeste do Brasil entre 2000 e 2017. *Cad. Geo.* **2021**, *31*, 546–556. [CrossRef]
15. Souza, E.O.; Costa, M.S.; Oliveira Júnior, J.F.; Gois, G.; Mariano, G.L.; Costa, C.E.D.S.; Santiago, D.B. Estimativa e Espacialização da Erosividade em Mesorregiões Climáticas no Estado de Alagoas. *Rev. Bras. Meteorol.* **2020**, *35*, 769–783. [CrossRef]
16. Tariq, A.; Yan, J.; Gagnon, A.S.; Riaz Khan, M.; Mumtaz, F. Mapping of cropland, cropping patterns and crop types by combining optical remote sensing images with decision tree classifier and random forest. *Geo-Spat. Inf. Sci.* **2022**, 1–19. [CrossRef]
17. Jalayer, S.; Sharifi, A.; Abbasi-Moghadam, D.; Tariq, A.; Qin, S. Modeling and Predicting Land Use Land Cover Spatiotemporal Changes: A Case Study in Chalus Watershed, Iran. *IEEE J. Sel. Top. Appl. Earth Obs. Remote Sens.* **2022**, *15*, 5496–5513. [CrossRef]
18. Ávila, P.L.R.; Brito, J.I.B. Relação entre a Oscilação Decadal do Pacífico e a variabilidade de precipitação de Campina Grande, PB. *Ciência E Nat.* **2015**, *37*, 159–162. [CrossRef]
19. Oliveira Júnior, J.F.; Correia Filho, W.L.F.; Monteiro, L.S.; Shah, M.; Hafeez, A.; Gois, G.; Lyra, G.B.; Abreu, M.C.; Santiago, D.D.B.; Souza, A.; et al. Urban rainfall in the Capitals of Brazil: Variability, trend, and wavelet analysis. *Atmos. Res.* **2022**, *267*, 105984. [CrossRef]
20. Wahla, S.S.; Kazmi, J.H.; Sharifi, A.; Shirazi, S.A.; Tariq, A.; Joyell Smith, H. Assessing spatio-temporal mapping and monitoring of climatic variability using SPEI and RF machine learning models. *Geocarto Int.* **2022**, 1–20. [CrossRef]
21. Tariq, A.; Mumtaz, F.; Zeng, X.; Baloch, M.Y.J.; Moazzam, M.F.U. Spatio-temporal variation of seasonal heat islands mapping of Pakistan during 2000–2019, using day-time and night-time land surface temperatures MODIS and meteorological stations data. *Remote Sens. Appl. Soc. Environ.* **2022**, *27*, 100779. [CrossRef]
22. Tariq, A.; Siddiqui, S.; Sharifi, A.; Hassan, S.; Ahmad, I. Impact of spatio-temporal land surface temperature on cropping pattern and land use and land cover changes using satellite imagery, Hafizabad District, Punjab, Province of Pakistan. *Arab. J. Geosci.* **2022**, *15*, 1045. [CrossRef]
23. Tariq, A.; Shu, H. CA-Markov chain analysis of seasonal land surface temperature and land use landcover change using optical multi-temporal satellite data of Faisalabad, Pakistan. *Remote Sens.* **2020**, *12*, 3402. [CrossRef]
24. Tariq, A.; Shu, H.; Gagnon, A.S.; Li, Q.; Mumtaz, F.; Hysa, A.; Siddique, M.A.; Munir, I. Assessing Burned Areas in Wildfires and Prescribed Fires with Spectral Indices and SAR Images in the Margalla Hills of Pakistan. *Forests* **2021**, *12*, 1371. [CrossRef]
25. Tariq, A.; Shu, H.; Kuriqi, A.; Siddiqui, S.; Gagnon, A.S.; Lu, L.; Linh, N.T.T.; Pham, Q.B. Characterization of the 2014 Indus River Flood Using Hydraulic Simulations and Satellite Images. *Remote Sens.* **2021**, *13*, 2053. [CrossRef]
26. Tariq, A.; Riaz, I.; Ahmad, Z. Land surface temperature relation with normalized satellite indices for the estimation of spatio-temporal trends in temperature among various land use land cover classes of an arid Potohar region using Landsat data. *Environ. Earth Sci.* **2020**, *79*, 40. [CrossRef]
27. Ahmad, A.; Ahmad, S.R.; Gilani, H.; Tariq, A.; Zhao, N.; Aslam, R.W.; Mumtaz, F. A Synthesis of Spatial Forest Assessment Studies Using Remote Sensing Data and Techniques in Pakistan. *Forests* **2021**, *12*, 1211. [CrossRef]
28. Hu, P.; Sharifi, A.; Tahir, M.N.; Tariq, A.; Zhang, L.; Mumtaz, F.; Shah, S.H.I.A. Evaluation of Vegetation Indices and Phenological Metrics Using Time-Series MODIS Data for Monitoring Vegetation Change in Punjab, Pakistan. *Water* **2021**, *13*, 2550. [CrossRef]
29. Sousa, F.D.A.S.; Vieira, V.R.; Vicente de Paulo, R.; Silva Melo, V.; Souza Guedes, R.W. Estimativas dos riscos de chuvas extremas nas capitais do Nordeste do Brasil. *Rev. Bras. Geo. Fis.* **2016**, *9*, 430–439. [CrossRef]
30. Da Silva, D.F.; Lima, M.J.S.; Souza Neto, P.F.; Gomes, H.B.; Silva, F.D.S.; Almeida, H.R.R.C.; Costa, R.L. Caracterização de eventos extremos e de suas causas climáticas com base no índice Padronizado de Precipitação Para o Leste do Nordeste. *Rev. Bras. Geo. Fis.* **2020**, *13*, 449–464. [CrossRef]
31. Mandú, T.B. Variabilidade da intensidade da precipitação no período chuvoso em Recife-PE. *Braz. J. Develop.* **2020**, *6*, 69045–69053.
32. IBGE—Instituto Brasileiro de Geografia e Estatística, 2022. Censos 2000 e 2010. Available online: https://ww2.ibge.gov.br/home/estatistica/populacao/censo2010/indicadores_sociais_municipais/ (accessed on 13 February 2022).
33. Harrel, F. *Regression Modeling Strategies: With Applications to Linear Models, Logistic Regression, and Survival Analysis*; Chapter 5: Resampling, Validating, and Simplifying the Model; Springer: Berlin/Heidelberg, Germany, 2001; Volume 3, pp. 88–103.
34. Junger, W.; Ponce de Leon, A. Mtsdi: Multivariate Time Series Data Imputation: R Package Version 0.3.5. 2018. Available online: <https://CRAN.R-project.org> (accessed on 20 April 2022).
35. Gois, G.; Freitas, W.K.; Terassi, P.M.B.; Oliveira-Júnior, J.F.; Portz, A. Variabilidade Anual e Mensal da Chuva e da Temperatura do Ar no Município de Resende, Rio de Janeiro. *Rev. Bras. Climatol.* **2019**, *24*, 67–88. [CrossRef]
36. Gois, G.; Oliveira-Júnior, J.F.; Silva Junior, C.A.; Sobral, B.S.; Terassi, P.M.B.; Leonel Junior, A.H.S. Statistical normality and homogeneity of a 71-year rainfall dataset for the state of Rio de Janeiro-Brazil. *Theor. Appl. Climatol.* **2020**, *141*, 1573–1591. [CrossRef]
37. NOAA/CPC—National Oceanic and Atmospheric Administration/Climate Prediction Center. Available online: http://www.cpc.ncep.noaa.gov/products/analysis_monitoring/ensostuff/ensoyears.shtml (accessed on 20 January 2022).
38. Mann, H.B. Nonparametric tests against trend. *Econom. J. Econom. Soc.* **1954**, *13*, 245–259. [CrossRef]
39. Kendall, M. *Rank Correlation Measures*; Charles Griffin: London, UK, 1975; Volume 202, p. 15.
40. Hänsel, S.; Medeiros, D.M.; Matschullat, J.; Petta, R.A.; de Mendonça Silva, I. Assessing homogeneity and climate variability of temperature and precipitation series in the capitals of north-eastern Brazil. *Front. Earth Sci.* **2016**, *4*, 29. [CrossRef]

41. Oliveira-Júnior, J.F.; Correia Filho, W.L.F.; Santiago, D.B.; Gois, G.; Costa, M.; Silva Junior, C.A.; Teodoro, P.E.; Freire, F.M. Rainfall in Brazilian Northeast via in situ data and CHELSA product: Mapping, trends, and socio-environmental implications. *Environ. Monit. Assess.* **2021**, *193*, 263–281. [[CrossRef](#)] [[PubMed](#)]
42. Jimenez, J.C.; Libonati, R.; Peres, L.F. Droughts over Amazonia in 2005, 2010, and 2015: A cloud cover perspective. *Front. Earth Sci.* **2018**, *6*, 227. [[CrossRef](#)]
43. Xie, X.; He, B.; Guo, L.; Huang, L.; Hao, X.; Zhang, Y.; Wang, S. Revisiting dry season vegetation dynamics in the Amazon rainforest using different satellite vegetation datasets. *Agric. For. Meteorol.* **2022**, *312*, 108704. [[CrossRef](#)]
44. Aragão, R.D.; Santana, G.R.D.; Da Costa, C.E.F.F.; Cruz, M.A.S.; Figueiredo, E.D.; Srinivasan, V.S. Chuvas intensas para o estado de Sergipe com base em dados desagregados de chuva diária. *Rev. Bras. Eng. Agríc. Amb.* **2013**, *17*, 243–252. [[CrossRef](#)]
45. Oliveira Júnior, J.F.; Lyra, G.B.; Gois, G.; Brito, T.T.; Moura, N.S.H. Análise de homogeneidade de séries pluviométricas para determinação do índice de seca IPP no estado de Alagoas. *Flor. Amb.* **2012**, *19*, 101–112. [[CrossRef](#)]
46. Oliveira Júnior, J.F.; Gois, G.; Silva, I.J.L.; Jardim, A.M.R.F.; Silva, M.V.; Shah, M.; Jamjareegulgarn, P. Wet and dry periods in the state of Alagoas (Northeast Brazil) via Standardized Precipitation Index. *J. Atmos. Sol. Terr. Phys.* **2021**, *224*, 105746. [[CrossRef](#)]
47. Rodrigues, E.L.; Lopes, R.F.C.; Sousa, F.A.S. Análise estatística da variabilidade da precipitação para o Município de João Pessoa-PB. *Braz. J. Dev.* **2021**, *7*, 73263–73271. [[CrossRef](#)]
48. Zhang, L.; Huang, M.; Li, M.; Lu, S.; Yuan, X.; Li, J. Experimental Study on Evolution of Fracture Network and Permeability Characteristics of Bituminous Coal Under Repeated Mining Effect. *Nat. Resour. Res.* **2021**, *31*, 463–486. [[CrossRef](#)]
49. Zhang, L.; Huang, M.; Xue, J.; Li, M.; Li, J. Repetitive Mining Stress and Pore Pressure Effects on Permeability and Pore Pressure Sensitivity of Bituminous Coal. *Nat. Resour. Res.* **2021**, *30*, 4457–4476. [[CrossRef](#)]
50. Gao, C.; Hao, M.; Chen, J.; Gu, C. Simulation and design of joint distribution of rainfall and tide level in Wuchengxiyu Region, China. *Urban Clim.* **2021**, *40*, 101005. [[CrossRef](#)]
51. Quan, Q.; Gao, S.; Shang, Y.; Wang, B. Assessment of the sustainability of *Gymnocypris eckloni* habitat under river damming in the source region of the Yellow River. *Sci. Total Environ.* **2021**, *778*, 146312. [[CrossRef](#)] [[PubMed](#)]
52. Zhang, K.; Wang, S.; Bao, H.; Zhao, X. Characteristics and influencing factors of rainfall-induced landslide and debris flow hazards in Shaanxi Province, China. *Nat. Hazards Earth Syst. Sci.* **2019**, *19*, 93–105. [[CrossRef](#)]
53. Pinheiro, J.M.; Araújo, R.R. Impactos do fenômeno El Niño e La Niña no município de São Luís-Maranhão. *Rev. GeoUECE* **2019**, *8*, 124–136.
54. Chaves, R.R.; Cavalcanti, I.F.A. Atmospheric circulation features associated with rainfall variability over southern Northeast Brazil. *Mon. Weather Rev.* **2001**, *129*, 2614–2626. [[CrossRef](#)]
55. Oliveira, D.H.M.C.; Lima, K.C. What is the return period of intense rainfall events in the capital cities of the northeast region of Brazil? *Atmos. Sci. Lett.* **2019**, *20*, e934. [[CrossRef](#)]
56. Uvo, C.R.B.; Berndtsson, R. Regionalization and Spatial Properties of Ceará State Rainfall in Northeast Brazil. *J. Geophys. Res. Atmos.* **1996**, *101*, 4221–4233. [[CrossRef](#)]
57. Kousky, V.E. Frontal influences on northeast Brazil. *Mon. Weather Rev.* **1979**, *107*, 1140–1153. [[CrossRef](#)]
58. Li, Z.; Zhang, K. Comparison of Three GIS-Based Hydrological Models. *J. Hydrol. Eng.* **2008**, *13*, 364–370. [[CrossRef](#)]
59. Xie, W.; Li, X.; Jian, W.; Yang, Y.; Liu, H.; Robledo, L.F.; Nie, W.A. Novel Hybrid Method for Landslide Susceptibility Mapping-Based GeoDetector and Machine Learning Cluster: A Case of Xiaojin County, China. *ISPRS Int. J. Geo-Inf.* **2021**, *10*, 93. [[CrossRef](#)]
60. Xie, W.; Nie, W.; Safari, P.; Robledo, L.F.; Descote, P.; Jian, W. Landslide hazard assessment based on Bayesian optimization-support vector machine in Nanping City, China. *Nat. Hazards* **2021**, *109*, 931–948. [[CrossRef](#)]
61. Zhu, Z.; Wu, Y.; Liang, Z. Mining-Induced Stress and Ground Pressure Behavior Characteristics in Mining a Thick Coal Seam with Hard Roofs. *Front. Earth Sci.* **2022**, *10*, 843191. [[CrossRef](#)]
62. Guo, Y.; Yang, Y.; Kong, Z.; He, J.; Wu, H. Development of Similar Materials for Liquid-Solid Coupling and Its Application in Water Outburst and Mud Outburst Model Test of Deep Tunnel. *Geofluids* **2022**, *2022*. [[CrossRef](#)]
63. Kousky, V.E. Diurnal rainfall variation in northeast Brazil. *Mon. Weather Rev.* **1980**, *108*, 488–498. [[CrossRef](#)]
64. Silva, V.P.R. On climate variability in Northeast of Brazil. *J. Arid Environ.* **2004**, *58*, 574–596. [[CrossRef](#)]
65. Correia Filho, W.L.F.; Oliveira-Júnior, J.F.; Santos, C.T.B.; Batista, B.A.; Barros Santiago, D.; Silva Junior, C.A.; Teodoro, P.E.; Costa, C.E.S.; Silva, E.B.; Freire, F.M. The influence of urban expansion in the socio-economic, demographic, and environmental indicators in the City of Arapiraca-Alagoas, Brazil. *Remote Sens. Appl. Soc. Environ.* **2022**, *25*, 100662. [[CrossRef](#)]
66. da Silva, M.V.; Pandorfi, H.; Jardim, A.M.D.R.F.; Oliveira-Júnior, J.F.; Divincola, J.S.; Giongo, P.R.; Silva, T.G.F.; Almeida, G.L.P.; Moura, G.B.A.; Lopes, P.M.O. Spatial modeling of rainfall patterns and groundwater on the coast of northeastern Brazil. *Urban Clim.* **2021**, *38*, 100911. [[CrossRef](#)]
67. Chen, Z.; Liu, Z.; Yin, L.; Zheng, W. Statistical analysis of regional air temperature characteristics before and after dam construction. *Urban Clim.* **2022**, *41*, 101085. [[CrossRef](#)]
68. Yin, L.; Wang, L.; Keim, B.D.; Konsoer, K.; Zheng, W. Wavelet Analysis of Dam Injection and Discharge in Three Gorges Dam and Reservoir with Precipitation and River Discharge. *Water* **2022**, *14*, 567. [[CrossRef](#)]
69. Yin, L.; Wang, L.; Zheng, W.; Ge, L.; Tian, J.; Liu, Y.; Liu, S. Evaluation of Empirical Atmospheric Models Using Swarm-C Satellite Data. *Atmosphere* **2022**, *13*, 294. [[CrossRef](#)]

70. Zhao, T.; Shi, J.; Lv, L.; Xu, H.; Chen, D.; Cui, Q.; Zhang, Z. Soil moisture experiment in the Luan River supporting new satellite mission opportunities. *Remote Sens. Environ.* **2020**, *240*, 111680. [[CrossRef](#)]
71. Zhao, T.; Shi, J.; Entekhabi, D.; Jackson, T.J.; Hu, L.; Peng, Z.; Kang, C.S. Retrievals of soil moisture and vegetation optical depth using a multi-channel collaborative algorithm. *Remote Sens. Environ.* **2021**, *257*, 112321. [[CrossRef](#)]
72. Chen, J.; Du, L.; Guo, Y. Label constrained convolutional factor analysis for classification with limited training samples. *Inf. Sci.* **2021**, *544*, 372–394. [[CrossRef](#)]
73. Li, Y.; Du, L.; Wei, D. Multiscale CNN Based on Component Analysis for SAR ATR. *IEEE Trans. Geosci. Remote Sens.* **2022**, *60*, 1–12. [[CrossRef](#)]
74. Liao, L.; Du, L.; Guo, Y. Semi-Supervised SAR Target Detection Based on an Improved Faster R-CNN. *Remote Sens.* **2021**, *14*, 143. [[CrossRef](#)]
75. Tian, H.; Qin, Y.; Niu, Z.; Wang, L.; Ge, S. Summer Maize Mapping by Compositing Time Series Sentinel-1A Imagery Based on Crop Growth Cycles. *J. Indian Soc. Remote Sens.* **2021**, *49*, 2863–2874. [[CrossRef](#)]
76. Tian, H.; Wang, Y.; Chen, T.; Zhang, L.; Qin, Y. Early-Season Mapping of Winter Crops Using Sentinel-2 Optical Imagery. *Remote Sens.* **2021**, *13*, 3822. [[CrossRef](#)]
77. Zhao, M.; Zhou, Y.; Li, X.; Cheng, W.; Zhou, C.; Ma, T.; Huang, K. Mapping urban dynamics (1992–2018) in Southeast Asia using consistent nighttime light data from DMSP and VIIRS. *Remote Sens. Environ.* **2020**, *248*, 111980. [[CrossRef](#)]
78. Zhao, M.; Zhou, Y.; Li, X.; Zhou, C.; Cheng, W.; Li, M.; Huang, K. Building a Series of Consistent Night-Time Light Data (1992–2018) in Southeast Asia by Integrating DMSP-OLS and NPP-VIIRS. *IEEE Trans. Geosci. Remote Sens.* **2020**, *58*, 1843–1856. [[CrossRef](#)]
79. Jiang, S.; Zuo, Y.; Yang, M.; Feng, R. Reconstruction of the Cenozoic tectono-thermal history of the Dongpu Depression, Bohai Bay Basin, China: Constraints from apatite fission track and vitrinite reflectance data. *J. Pet. Sci. Eng.* **2021**, *205*, 108809. [[CrossRef](#)]
80. Zuo, Y.; Jiang, S.; Wu, S.; Xu, W.; Zhang, J.; Feng, R.; Santosh, M. Terrestrial heat flow and lithospheric thermal structure in the Chagan Depression of the Yingen-Ejinaqi Basin, north central China. *Basin Res.* **2020**, *32*, 1328–1346. [[CrossRef](#)]
81. Zhang, Z.; Luo, C.; Zhao, Z. Application of probabilistic method in maximum tsunami height prediction considering stochastic seabed topography. *Nat. Hazards* **2020**, *104*, 2511–2530. [[CrossRef](#)]